Adjoint-based unsteady optimization of turbomachinery operating with nonideal compressible flows

Rubino, Antonio; Colonna, Piero; Pini, Matteo

DOI
10.2514/1.B37920

Publication date
2021

Document Version
Final published version

Published in
Journal of Propulsion and Power

Citation (APA)
Rubino, A., Colonna, P., & Pini, M. (2021). Adjoint-based unsteady optimization of turbomachinery operating with nonideal compressible flows. *Journal of Propulsion and Power*, *37*(6), 910-918. https://doi.org/10.2514/1.B37920

JOURNAL OF PROPULSION AND POWER
Vol. 37, No. 6, November–December 2021

Adjoint-Based Unsteady Optimization of Turbomachinery Operating with Nonideal Compressible Flows

Antonio Rubino,* Piero Colonna,† and Matteo Pini‡
Delft University of Technology, 2629 HS Delft, The Netherlands

https://doi.org/10.2514/1.B37920

The lack of established optimal design guidelines for turbomachinery operating in the nonideal flow regime (e.g., organic Rankine cycle turbines, CO_2 compressors, compressors for refrigeration systems) demands for effective and efficient automated design methods. Past research work focused on gradient-free methods applied to computational fluid-dynamic simulations. The application of the adjoint method is a cost-effective alternative as it enables gradient-based optimization irrespective of the number of design variables. This paper presents the application of a fully turbulent unsteady adjoint method for the automated design of multirow turbomachinery partly operating in the nonideal flow regime. The method therefore allows for the solution of constrained unsteady fluid-dynamic optimization problems, in which the thermodynamic properties of the working fluid need to be modeled by means of complex equations of state. The optimal designs computed with unsteady simulations obtained with the harmonic balance method are then compared with optimal design resulting from mixing-plane simulations. The method is applied to the optimization of 1) a two-dimensional turbine cascade subject to time-varying inlet conditions, and 2) a two-dimensional turbine stage of an organic Rankine cycle power system. The results demonstrate the importance of computing fluid properties using accurate thermodynamic models and of using unsteady simulations for shape optimization of these machines.

I. Introduction

TURBOMACHINERY components are fundamental in the aviation, automotive, and energy industry, to name a few. Diverse engineering applications require turbomachinery operating with nonideal compressible fluid flows, i.e., flows of fluids whose thermodynamic properties cannot be modeled according to the ideal gas assumption, but require complex equations of state. Examples of such applications include compressors of supercritical CO_2 power plants, turbines of organic Rankine cycle (ORC) power systems, compressors for refrigeration systems, and steam turbines [1–4].

For these turbomachines, the shortage of experimental data and accurate loss models entails an absence of optimal design guidelines, especially for new and unconventional applications. In such cases, a viable solution is to obtain a preliminary design with methods originally developed for conventional turbines and compressors. However, because of the underlying assumptions, these models can lead to attain highly suboptimal designs. The obtained preliminary design can then be optimized, but it is crucial that the optimization method is capable of taking into account nonideal compressible fluid-dynamic effects. This requirement makes the complexity of the method and the computational effort even more challenging. Thanks to the advancements in computational resources, these methods are becoming more and more a viable option, offering the possibility to improve current components performance and to explore innovative solutions.

Past work in the area of automated shape optimization of turbomachinery operating with nonideal compressible flows has focused on both nondeterministic and deterministic methods. Nondeterministic methods have been successfully applied, for example, to the constrained optimization of ORC turbine cascades [5–7]. These methods are robust if dealing with nonsmooth objective functions and are suitable for global optimization. However, their computational cost can become prohibitive if a large set of design variables (DVs) has to be considered and if fluid properties must be evaluated with complex thermodynamic models. Deterministic (gradient-based) algorithms are in general very efficient in converging to optimal solutions, but they require the evaluation of the gradients of the objective function. The objective function must, therefore, feature regularity properties and the gradient estimation must be computationally inexpensive. In this respect, adjoint-based algorithms provide an efficient way to compute design gradients for deterministic optimization methods.

Recently, adjoint-based shape optimization methods have been extended to treat also turbomachinery affected by strong nonideal compressible fluid dynamics (NICFD) effects [8]. With these algorithms it is possible to perform automated design very efficiently if the number of DVs is much larger than the number of objective functions or constraints. For this reason, adjoint-based optimization methods are a very attractive, and sometimes necessary, alternative to nondeterministic algorithms for CFD-based turbomachinery design. To date, however, adjoint-based turbomachinery optimization involving nonideal compressible flows has been successfully applied only to single cascades and under the assumption that the flow is stationary [8,9]. In the very recent past, the method has been extended to the optimization of multirow machines [10].

This paper documents an adjoint-based turbomachinery design optimization method relying on fully turbulent unsteady flow simulations and capable of treating nonideal compressible flows. The optimization algorithm implemented in the SU2 open-source code [11,12] and based on the harmonic balance (HB) method documented in Refs. [13,14] was extended to include the possibility of estimating fluid thermodynamic properties with complex models. The thermodynamic properties of the fluid are obtained either with a cubic equation of state model coded in SU2, or by interpolating data from ad hoc tables [15] generated with an external fluid property library [16]. The corresponding adjoint equations are obtained by applying algorithmic differentiation to the SU2 source code in a black-box fashion. The method is first applied to the computation and verification of the design sensitivities of a two-dimensional turbine cascade, in order to test its capabilities and validity. Subsequently, the constrained shape optimization of a two-dimensional ORC turbine stage is performed to demonstrate its potential in a realistic case.

Received 2 December 2019; revision received 1 April 2021; accepted for publication 1 April 2021; published online Open Access 14 July 2021.

*Researcher, Propulsion and Power, Aerospace Engineering Faculty, Kluyverweg 1.
†Full Professor, Propulsion and Power, Aerospace Engineering Faculty, Kluyverweg 1.
‡Assistant Professor, Propulsion and Power, Aerospace Engineering Faculty, Kluyverweg 1.

II. Method

A. Flow Model

Let ρ be the density; E the total energy per unit mass defined as $E = e + 1/2|\boldsymbol{v}\cdot\boldsymbol{v}$, with e the specific internal energy; t time; and $\boldsymbol{v}$ the velocity vector in a Cartesian frame of reference. From the differential form of the Navier–Stokes equations

$$\frac{\partial \boldsymbol{U}}{\partial t} + \nabla\cdot\boldsymbol{F}^{\boldsymbol{c}} - \nabla\cdot\boldsymbol{F}^{\boldsymbol{v}} = 0 \text{ in } \Omega, t > 0 \tag{1}$$

the following semidiscrete form can be written as

$$\Omega\frac{\partial \boldsymbol{U}}{\partial t} + \mathcal{R}(\boldsymbol{U}) = 0, t > 0 \tag{2}$$

$\boldsymbol{U} = (\rho, \rho v_1, \rho v_2, \rho v_3, \rho E)$ is the vector of conservative variables and $\mathcal{R}$ the residual operator applied to the spacial integration of the convective and viscous fluxes $\boldsymbol{F}^{\boldsymbol{c}}$ and $\boldsymbol{F}^{\boldsymbol{v}}$. The application of an arbitrary Lagrangian–Eulerian (ALE) formulation on the domain Ω, moving with velocity $\boldsymbol{u}_\Omega$ without deforming in time, and its boundary $\partial\Omega$ [17] results in

$$\mathcal{R}(\boldsymbol{U}) = f(\boldsymbol{F}^{\boldsymbol{c}}, \boldsymbol{F}^{\boldsymbol{v}}) \text{ in } \Omega, t > 0, \quad \boldsymbol{v} = \boldsymbol{u}_\Omega \text{ on } \partial\Omega, t > 0 \tag{3}$$

The convective fluxes are

$$\boldsymbol{F}^{c} = \begin{pmatrix} \rho(\boldsymbol{v} - \boldsymbol{u}_\Omega) \\ \rho\boldsymbol{v}\times(\boldsymbol{v} - \boldsymbol{u}_\Omega) + p\bar{\boldsymbol{I}} \\ \rho E(\boldsymbol{v} - \boldsymbol{u}_\Omega) + p\boldsymbol{v} \end{pmatrix} \tag{4}$$

and the viscous fluxes are

$$\boldsymbol{F}^{v} = \begin{pmatrix} 0 \\ \bar{\boldsymbol{\tau}} \\ \bar{\boldsymbol{\tau}}\cdot\boldsymbol{v} - \kappa\nabla T \end{pmatrix} \tag{5}$$

Here, p and T are the static pressure and temperature, κ is the thermal conductivity, μ is the dynamic viscosity, and $\bar{\boldsymbol{\tau}}$ is the viscous stress tensor

$$\bar{\boldsymbol{\tau}} = \mu(\nabla\boldsymbol{v} + \nabla\boldsymbol{v}^{\intercal}) - \frac{2}{3}\mu\bar{\boldsymbol{I}}(\nabla\cdot\boldsymbol{v}) \tag{6}$$

For unsteady Reynolds-Averaged Navier-Stokes (RANS) equations, according to the Boussinesq hypothesis, the turbulence modeling is accounted for by defining $\mu = \mu_l + \mu_t$, and $\kappa = \kappa_l + \kappa_t$, where μ_l and μ_t are the laminar and turbulent dynamic viscosities, whereas κ_l and κ_t are the laminar and turbulent thermal conductivities; κ_t is computed assuming a constant value of the turbulent Prandtl number Pr_t. The dependence of μ from the static temperature T is neglected. The vector of the conservative variables $\boldsymbol{U}$ for RANS can be redefined as

$$\boldsymbol{U} \coloneqq \begin{pmatrix} \boldsymbol{U}_l \\ \boldsymbol{U}_t \end{pmatrix}, \qquad \mathcal{R}(\boldsymbol{U}) = \mathcal{R}(\boldsymbol{U}_f, \boldsymbol{U}_t) \coloneqq \begin{pmatrix} \mathcal{R}_f(\boldsymbol{U}_l, \boldsymbol{U}_t) \\ \mathcal{R}_t(\boldsymbol{U}_l, \boldsymbol{U}_t) \end{pmatrix} \tag{7}$$

in which $\boldsymbol{U}_l = (\rho, \rho v_1, \rho v_2, \rho v_3, \rho E)$ and $\boldsymbol{U}_t$ is the vector of the conservative variables associated to the selected turbulence model. For example, in case of the Menter shear stress transport (SST) model [18], $\boldsymbol{U}_t = (\rho\kappa, \rho\omega)$, with κ the turbulent kinetic energy and ω the specific dissipation.

In analogy with the treatment described in [13], after time-integration and linearization of the residual operator and applying the harmonic balance method with dual-time stepping of pseudotime τ, one can obtain the following discretized expression for the RANS equations

$$\left(\frac{\Omega\boldsymbol{I}}{\Delta\tau} + \boldsymbol{J}\right)\Delta\boldsymbol{U}_n = -\widehat{\mathcal{R}}_n(\boldsymbol{U}^q), \qquad n = 0, 1, \ldots, N-1 \tag{8}$$

in which

$$\widehat{\mathcal{R}}_n(\boldsymbol{U}^q) = \mathcal{R}_n(\boldsymbol{U}^q) + \Omega\sum_{i=0}^{N-1} H_{n,i}\Delta\boldsymbol{U}_i + \Omega\sum_{i=0}^{N-1} H_{n,i}\boldsymbol{U}_i^q \tag{9}$$

In Eq. (9), n refers to a specific time instance, q indicates the pseudotime stepping, and $\boldsymbol{H}$ is the harmonic balance operator, calculated for a known set of K input frequencies and corresponding to $N = 2K + 1$ time instances, written as

$$\boldsymbol{H} = \begin{pmatrix} H_{1,1} & H_{1,2} & \cdots & H_{1,N} \\ H_{2,1} & H_{2,2} & \cdots & H_{2,N} \\ \vdots & \vdots & \ddots & \vdots \\ H_{N,1} & H_{N,2} & \cdots & H_{N,N} \end{pmatrix} \tag{10}$$

$\boldsymbol{H}$ is the result of the following matrix product:

$$\boldsymbol{H} = \boldsymbol{E}^{-1}\boldsymbol{D}\boldsymbol{E} \tag{11}$$

$\boldsymbol{E}$ and $\boldsymbol{E}^{-1}$ are the direct and inverse Fourier matrix, and $\boldsymbol{D}$ is the diagonal matrix containing the K input frequencies, i.e., $\boldsymbol{D} = \text{diag}(0, i\omega_1, \ldots, i\omega_K, -i\omega_{-K}, \ldots, -i\omega_1)$. $\boldsymbol{U}$ indicates here the vector of conservative variables and includes both laminar and turbulent quantities.

In RANS solvers for nonideal compressible flows, the fluid properties are calculated with arbitrary equations of state, by either using polytropic models, e.g., the polytropic ideal gas model or the polytropic Peng–Robinson (PR) model, or via lookup tables [15]. As an illustrative example, the equations formulating the polytropic PR model in its natural variables T and $v = 1/\rho$ are listed in Appendix. The implementation of the thermodynamic model is based on equations featuring diverse thermodynamic couples, e.g., ρ, e or p, s, where s is the specific entropy, as independent variables that can be obtained from its original formulation by simple algebraic derivation or numerical resolution. The transport properties are instead assumed to be constant. This is because common viscosity models for the fluids considered in this work are affected by uncertainty of the order of 30%, and as such the accuracy that one can attain by adopting a constant viscosity model (computed, e.g., as algebraic average between the value at inlet and the value at outlet conditions) is usually sufficient for design purposes.

B. Fully Turbulent Discrete Adjoint and Nonideal Compressible Flows

The adjoint equations are derived by making the dependence of the vector of conservative variables $\boldsymbol{U}$ from the vector of primitive variables $\Theta = [\rho, e, \boldsymbol{v}]$ explicit, where $\boldsymbol{v}$ is the velocity vector. The vector of turbulent quantities is herein omitted for simplicity. Note that the computation of the laminar part of $\boldsymbol{U}$ from Θ requires the calculation of the primary and secondary thermodynamic variables through an equation of state model, as documented in [15]. This explicit dependence allows one to outline the additional sensitivities arising in the gradient equation for nonideal compressible flows that can be computed only by differentiating a complex thermodynamic model or tabulation method.

Application of the fixed-point iteration method to Eq. (8) results in

$$\boldsymbol{U}_{z,n}^{q+1} = \mathcal{G}_{z,n}(\boldsymbol{U}_{z,n}^{q}) \tag{12}$$

in which $\boldsymbol{U}_{z,n}$ and $\mathcal{G}_{z,n}$ are the vector of conservative variables and the iteration operator of the pseudotime stepping relative to the physical zone z and for time instance n. Each physical zone z corresponds to a blade row.

By specifying the dependence of $\boldsymbol{U}_{z,n}$ from the set of DVs $\boldsymbol{\alpha}_z$ and the thermodynamic model Θ, the optimization problem can be written as

$$\begin{aligned}
&\underset{\boldsymbol{\alpha}_z}{\text{minimize}} \quad \mathcal{J}(\Theta(\boldsymbol{\alpha}_z, \boldsymbol{U}), X(\boldsymbol{\alpha}_z)) \\
&\text{subject to} \quad \Theta_{z,n}(\boldsymbol{\alpha}_z, \boldsymbol{U}_{z,n}) = \mathcal{G}_{z,n}(\Theta_{z,n}(\boldsymbol{\alpha}_z, \boldsymbol{U}_{z,n}), X_{z,n}(\boldsymbol{\alpha}_z)), \\
&\qquad\qquad n = 0, 1, \ldots, N-1 \quad z = 0, 1, \ldots, Z-1 \\
&\qquad\qquad X_{z,n}(\boldsymbol{\alpha}_z) = \mathcal{M}_z(\boldsymbol{\alpha}_z)
\end{aligned} \tag{13}$$

$\mathcal{J}$ is a generic objective function, $X_{z,n}$ is the physical grid for each zone and time instance, and $\mathcal{M}_z$ is a differentiable function representing the mesh deformation algorithm. The objective function $\mathcal{J}$, as shown in [13], is computed as a time average by applying Fourier interpolation of the resolved time instances.

The Lagrangian of the optimization problem is

$$\begin{aligned}
\mathcal{L} = \mathcal{J} + \sum_{z=0}^{Z-1}\sum_{n=0}^{N-1}((\mathcal{G}_{z,n}(\Theta_{z,n}(\boldsymbol{\alpha}_z, \boldsymbol{U}_{z,n}), X_{z,n}(\boldsymbol{\alpha}_z)) - \Theta_{z,n}(\boldsymbol{\alpha}_z, \boldsymbol{U}_{z,n}))^\intercal \boldsymbol{\lambda}_{z,n}) \\
+ (\mathcal{M}_z(\boldsymbol{\alpha}_z) - X_{z,n}(\boldsymbol{\alpha}_z))^\intercal \boldsymbol{\mu}_z
\end{aligned} \tag{14}$$

with $\boldsymbol{\lambda}$ and $\boldsymbol{\mu}$ being the adjoint variables. The differential of the Lagrangian is

$$\begin{aligned}
d\mathcal{L} = &\sum_{z=0}^{Z-1}\sum_{n=0}^{N-1}\left(\frac{\partial\Theta_{z,n}^\intercal}{\partial \boldsymbol{U}_{z,n}}\frac{\partial\mathcal{J}^\intercal}{\partial\Theta_{z,n}} + \sum_{i=0}^{Z-1}\sum_{j=0}^{N-1}\frac{\partial\Theta_{z,n}^\intercal}{\partial \boldsymbol{U}_{z,n}}\frac{\partial\mathcal{G}_{i,j}^\intercal}{\partial\Theta_{i,j}}\boldsymbol{\lambda}_{i,j} - \boldsymbol{\lambda}_{z,n}\right) d\boldsymbol{U}_{z,n} \\
&+ \sum_{z=0}^{Z-1}\sum_{n=0}^{N-1}\left(\frac{\partial\mathcal{J}^\intercal}{\partial X_{z,n}} + \frac{\partial\mathcal{G}_{z,n}^\intercal}{\partial X_{z,n}}\boldsymbol{\lambda}_{z,n}\right) dX_{z,n} - \boldsymbol{\mu}_z dX_{z,n} \\
&+ \sum_{z=0}^{Z-1}\frac{\partial\mathcal{M}_z^\intercal}{\partial\boldsymbol{\alpha}_z}\boldsymbol{\mu}_z d\boldsymbol{\alpha}_z
\end{aligned} \tag{15}$$

from which the adjoint equations can be derived as

$$\frac{\partial\Theta_{z,n}^\intercal}{\partial \boldsymbol{U}_{z,n}}\frac{\partial\mathcal{J}^\intercal}{\partial\Theta_{z,n}} + \sum_{i=0}^{Z-1}\sum_{j=0}^{N-1}\frac{\partial\Theta_{z,n}^\intercal}{\partial \boldsymbol{U}_{z,n}}\frac{\partial\mathcal{G}_{i,j}^\intercal}{\partial\Theta_{i,j}}\boldsymbol{\lambda}_{i,j} = \boldsymbol{\lambda}_{z,n} \tag{16}$$

and

$$\frac{\partial\mathcal{J}^\intercal}{\partial X_{z,n}} + \frac{\partial\mathcal{G}_{z,n}^\intercal}{\partial X_{z,n}}\boldsymbol{\lambda}_{z,n} = \boldsymbol{\mu}_z \tag{17}$$

$\boldsymbol{\mu}_z$ is directly computed from Eq. (17) given the solution $\boldsymbol{\lambda}_{zn}$ of Eq. (16). In analogy to the flow solver, Eq. (16) can be expressed as a fixed-point iteration in $\boldsymbol{\lambda}_{z,n}$:

$$\boldsymbol{\lambda}_{z,n}^{q+1} = \frac{\partial\mathcal{N}}{\partial \boldsymbol{U}_{z,n}}(\boldsymbol{U}_{z,n}^*, \boldsymbol{\lambda}^q, X_{z,n}) \tag{18}$$

where $\boldsymbol{U}_n^*$ is the solution of Eq. (12) and $\mathcal{N}$ is the shifted Lagrangian defined as

$$\mathcal{N} = \mathcal{J} + \sum_{z=0}^{Z-1}\sum_{n=0}^{N-1}\mathcal{G}_{z,n}^\intercal(\boldsymbol{U}, X_{z,n})\boldsymbol{\lambda}_{z,n} \tag{19}$$

The gradient of the objective function $\mathcal{J}$ with respect to the vector of the DVs $\boldsymbol{\alpha}_z$ can be computed, for each numerical zone, from the converged flow and adjoint solutions using

$$\frac{d\mathcal{L}^\intercal}{d\boldsymbol{\alpha}_z} = \frac{d\mathcal{J}^\intercal}{d\boldsymbol{\alpha}_z} = \frac{\partial\mathcal{M}_z(\boldsymbol{\alpha}_z)^\intercal}{\partial\boldsymbol{\alpha}_z}\boldsymbol{\mu}_z \qquad z = 0, 1, \ldots, Z-1 \tag{20}$$

Figure 1 reports a schematic representation summarizing the design chain procedure. The term $\partial\Theta/\partial\boldsymbol{U}$ contains the derivation of the tabulation (lookup table) method. All the derivatives needed to solve Eq. (18) are obtained by means of algorithmic differentiation (AD). As opposed to the approach documented in [9], the reverse mode of the open-source AD tool CoDiPack [19] was used to linearize the primal solver along with the equation of state model in a fully black-box manner. For turbomachinery design problems in which fluid-dynamic losses are to be minimized, the objective function $\mathcal{J}$ is usually expressed as entropy generation or total pressure loss coefficient. The minimization of entropy generation is documented here.

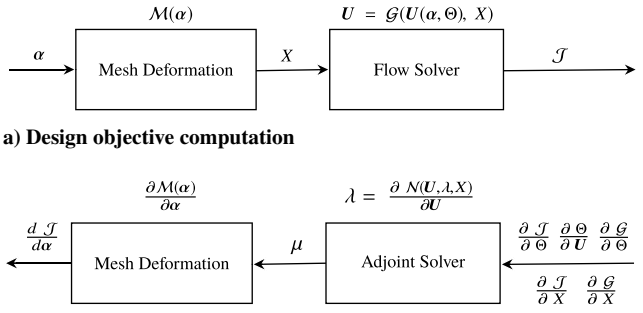

Fig. 1 Schematic representation of the design problem.

III. Adjoint-Based Optimization Using Lookup Tables

The adjoint-based gradients of the entropy generation are computed for the turbine cascade described in [15], using the same physical model, i.e., RANS with SST-$k\omega$ turbulence model, boundary conditions and working fluid (siloxane MDM). The convective fluxes are discretized by a generalized Roe scheme, and second-order accuracy is achieved with the MUSCL approach. The hybrid mesh comprises about 50k elements to ensure $y^+ \approx 1$. The main simulation parameters are reported in Table 1.

Differently from what reported in [15], a time-varying total pressure $\tilde{P}_{\text{tot}}$ is imposed at the inlet of the cascade according to

$$\tilde{P}_{\text{tot}} = P_{\text{tot}}[1 + A\sin(2\pi t^*)] \tag{21}$$

in which $A = 0.03$, $t^* = t/T_0$, and $P_{\text{tot}} = P_r P_c$, where P_c is the critical pressure of the fluid. The amplitude and the frequency of the time-varying total inlet pressure have been selected based on typical values of the pitchwise pressure fluctuations downstream of transonic ORC turbine cascades. The shape optimization is performed using the HB method in combination with the lookup table method (ug-LUT) described in [15]. A thermodynamic grid composed of 10,000 mesh elements was found to be sufficient to accurately compute the fluid properties by using a bilinear interpolation method. Figure 2 shows the free-form deformation (FFD) box adopted for the turbine blade and the corresponding set of 12 control points. The control points are bounded to move in the y direction; therefore $\boldsymbol{\alpha}$ consists of 12 DVs. To quantify the unsteady fluid-dynamic performance of the stator, the dimensionless entropy generated in the flow passage of the stator is considered and calculated as

$$s_{\text{gen}} = \frac{\langle s_{\text{out}}\rangle - \langle s_{\text{in}}\rangle}{v_0^2/T_{0,\text{in}}} \tag{22}$$

Here, $\langle s_{\text{out}}\rangle$ and $\langle s_{\text{in}}\rangle$ are the outlet and inlet entropy averaged over the respective boundaries using the mixed-out procedure [20]; v_0 is the

Table 1 Main simulation parameters of the axial turbine cascade

Parameter	Value	Unit
Total inlet reduced temperature T_r	1.05	—
Total inlet reduced pressure P_r	1.05	—
Expansion ratio	1.26	—
Inlet turbulent intensity	5%	—
Turbulent viscosity ratio	100	—
Dynamic viscosity	1.3764×10^{-5}	kg/(m · s)
Thermal conductivity	0.047280	W/(m · K)

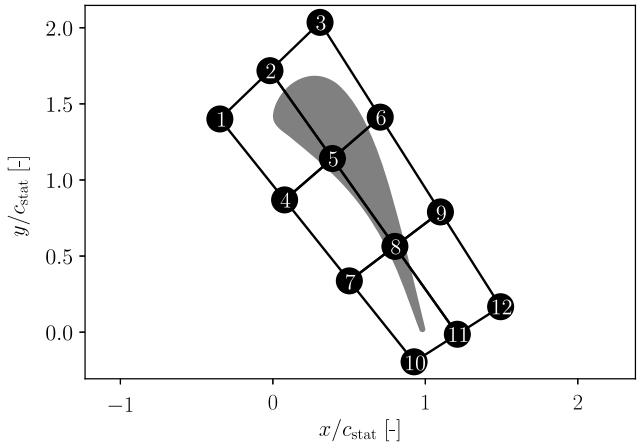

Fig. 2 LS-89 turbine cascade blade geometry, FFD box, and control points. The control points can only move in the *y* direction.

spout velocity; and $T_{0,\text{in}}$ the inlet total temperature. For the case at hand, the HB simulation results are obtained by using one frequency, namely, the main frequency of those considered in Eq. (21). As shown in Ref. [15], one harmonic is sufficient for unsteady subsonic design problems, in which the external excitation is characterized by a single frequency. All the single quantities used in Eq. (22) are computed as the time-averaged values of the resolved time instances.

The adjoint-based gradients obtained from the simulations in which the fluid properties are computed using the ug-LUT method are denoted for simplicity as LUT. The tabulated thermodynamic properties were computed through an accurate, thus complex, model based on an equation of state in the Span–Wagner functional form available in [16]. Furthermore, LUT-AD and LUT-FD refer to the sensitivities calculated using the adjoint method and finite differences, respectively. To verify the results, the adjoint-based design gradients are compared with those obtained by employing second-order-accurate finite differences (Fig. 3). The figure shows the design sensitivities in the *y* direction as calculated by the two methods. It can be seen that there is generally a good agreement and that the deviation between the two values increases when the sensitivities assume very low values, arguably a result of the larger truncation errors inherent to both methods. The root mean square error (RMSE) between the gradients from LUT-AD and LUT-FD is approximately 0.021.

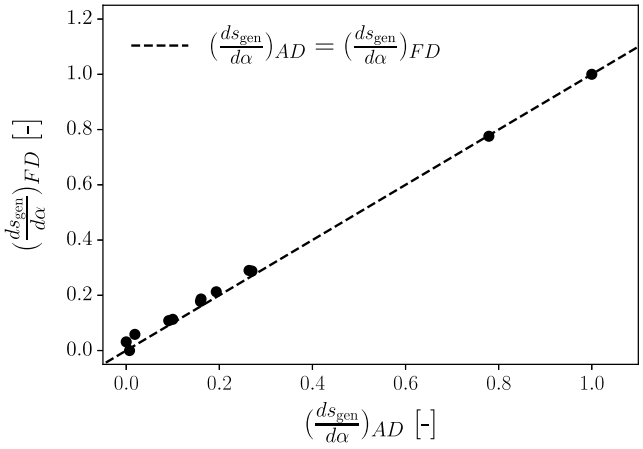

Fig. 3 Adjoint-based (AD) vs second-order finite differences (FD) design gradients.

Figure 4 displays the gradients with respect to the DVs obtained from LUT-AD and LUT-FD, relative to the DVs reported in Fig. 2. Moreover, it reports the adjoint-based gradients from the simulation in which the ideal gas equation of state is adopted to model the fluid properties (IG). The relative difference of the values of the design sensitivities in the *y* direction calculated with LUT and those calculated with IG is in excess of 20% for most DVs (Fig. 5) and up to 110% for the DVs located in proximity of the blade trailing edge (TE) (Fig. 4).

Table 2 reports the computational performance of the primal and adjoint solver with the PR and LUT models relative to the ones of the flow solver in which the IG model is used. The runtime per iteration of the adjoint solver is on average 30% higher than the one of the direct solver for all thermodynamic models, and it requires about four times more memory usage.

The verified adjoint-based gradients are finally used to perform the constrained shape optimization of the illustrative transonic turbine cascade. The selected gradient-based optimization algorithm is the modified version of the nonlinear least-squares method (SLSQP) [21].

The constrained optimization problem is formulated as

$$\begin{aligned} &\underset{\boldsymbol{\alpha}}{\text{minimize}} \quad s_{\text{gen}}(\boldsymbol{\alpha}), \\ &\text{subject to:} \quad \beta_{\text{out}} = \beta_{\text{out},0} \end{aligned} \tag{23}$$

in which β_{out} is the outlet flow angle with the correspondent constrained nominal value β_{out}.

The results of the blade shape optimizations are termed "LUT" if fluid properties are obtained from lookup tables, and "PR" if properties are calculated with the PR model implemented in SU2. Figure 6 shows the optimized shapes highlighting, therefore, the differences. The convergence to the optimal solution of the constrained optimization problem, expressed as relative change of the value of both the objective function and the constraint over the last three design steps, is lower than a specified tolerance. When selecting a tolerance of 10^{-3}, the optimal solution is reached after 14 iterations, as depicted in Fig. 7. The final results are summarized in Table 3. The results reported in Table 3 relative to the PR-based optimization are computed by running LUT and using the optimized shape from PR. The LUT-based design leads to a decrease in entropy generation by approximately 19.2%, whereas a decrease by about 12.0% if PR is used. For both optimizations, the constraint is met with a deviation below 0.05% with respect to the baseline outlet flow angle.

Figure 8a reports the loss breakdown in terms of the kinetic energy loss coefficient of the cascade, computed according to the procedure indicated in [22]. The optimization based on LUT results in lower TE losses and comparable boundary-layer (BL) loss if compared with the PR-based design, thus resulting in overall better fluid-dynamic performance. The reason of the higher TE losses induced by the PR-based optimized blade is found to be attributed to the inability of the PR model to resolve accurately the BL state close to the TE as a result

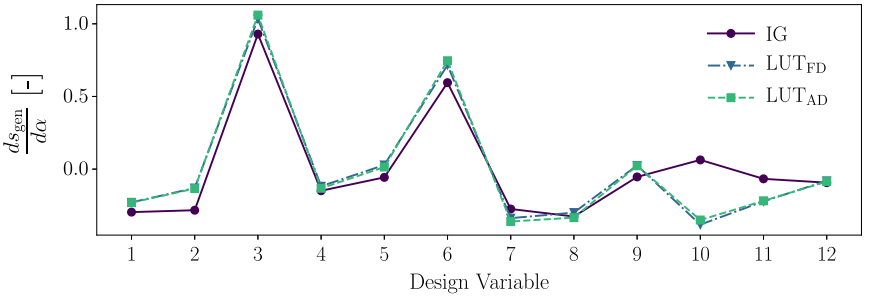

Fig. 4 Entropy generation gradients relative to the FFD box design variables (Fig. 2) obtained from LUT-AD, LUT-FD, and IG.

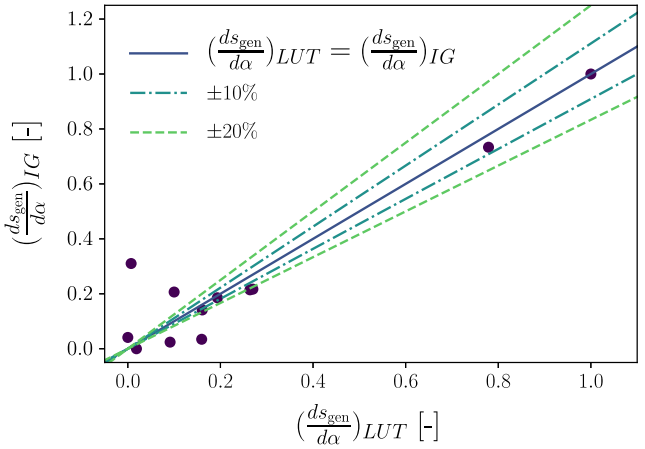

Fig. 5 Adjoint-based design sensitivities in *y* direction calculated with the LUT and IG model.

Table 2 Computational performance per iteration of the primal and adjoint solver with different thermodynamic models relative to the performance of the flow solver with the IG model

Primal	IG	PR	LUT
Runtime	1	1	1.05
Memory	1	1	1.1
Adjoint	IG	PR	LUT
Runtime	1.3	1.3	1.3
Memory	4.0	4.0	4.0

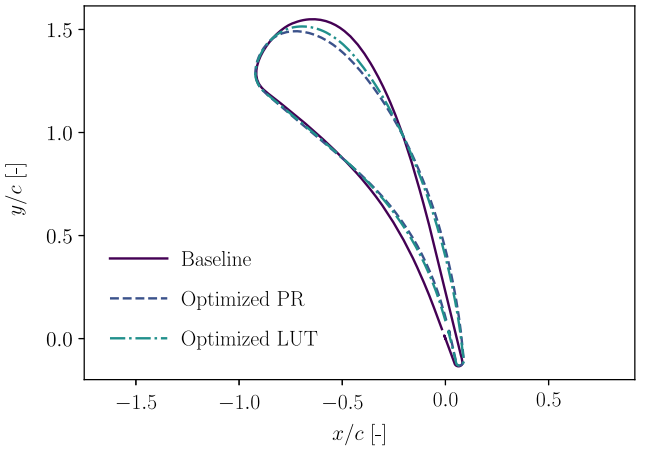

Fig. 6 Shape optimization results for the LS-89 cascade, obtained from IG, PR, and LUT.

of the inaccurate prediction of the suction surface velocity distribution. This leads to an underestimation of the base pressure coefficient [23,24] and thus TE losses, relative to the optimized blade if the properties are computed with LUT. These findings show that the use of an accurate equation of state is essential to optimize turbine cascades operating in the nonideal flow regime as this can enable a considerable attenuation of loss mechanisms occurring when the fluid already reached ideal gas states. Figure 8b displays the isentropic Mach number distribution along the baseline and LUT-based optimized blade. The largest discrepancies are located on the suction side, where the profile of the optimized blade is characterized by a velocity peak followed by a recompression and an eventual flow acceleration just before the TE. A more pronounced flow acceleration can instead be observed on the rear pressure side. While viscous dissipation on the blade walls is relatively insensitive to the change of the pressure profile, the TE losses reduce, arguably due to the lower momentum thickness of the accelerating BL upstream of the TE of the optimized blade.

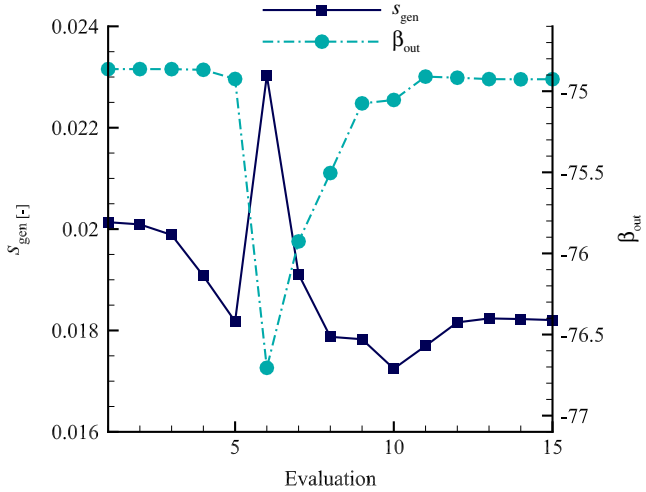

Fig. 7 Convergence history of the optimization process of the LS-89 cascade.

Table 3 LS89 turbine cascade optimization results

Quantity	Baseline	PR optimization	LUT optimization
s_{gen}	0.020	0.018	0.017
β_{out} [°]	74.86	74.88	74.89
$\delta_{s_{gen}}$	0.00%	−12.0%	−19.2%
$\delta_{\beta_{out}}$	0.00%	+0.03%	+0.04%

Figure 9 shows the Mach number contours obtained from HB simulations of the flow around the baseline and the LUT-based optimized geometries at the first time instance. The reduction of TE losses in the optimized configuration can be attributed to a mitigation of the velocity differences, i.e., the shear stresses, between the wake and the bulk flow, which eventually leads to a decrease of mixing losses. As the cascades operate in the transonic regime, the onset of a shock wave on the suction side weakly affects the BL losses in the optimized case.

IV. Shape Optimization of an Axial ORC Turbine Stage

The test case described here represents an exemplary stage of ORC turbines, with the stator operating in the nonideal compressible fluid-dynamic regime. The stage is characterized by the following isentropic design parameters: flow coefficient $\phi = 0.55$, work coefficient $\lambda = 1.1$, and degree of reaction $R = 0.4$. The working fluid is refrigerant $R1234yf$. The constrained shape optimization problem of the axial stage depicted in Fig. 13 is performed according to the following formulation:

$$\begin{aligned} &\underset{\boldsymbol{\alpha}_i}{\text{minimize}} \quad s_{gen}(\boldsymbol{\alpha}_i), \qquad i = 1, 2 \\ &\text{subject to:} \quad P^* > P_0^* \end{aligned} \tag{24}$$

in which P^* is the dimensionless power of the stage defined as

$$P^* = \frac{w\dot{m}}{\rho_{0,in} y_p u_b^3} \tag{25}$$

Here, w is the specific work, $\dot{m}$ the mass flow rate based on the blade pitch y_p, $\rho_{0,in}$ the total density at the stage inlet, and u_b the blade speed. Table 4 reports the main simulation parameters.

A hybrid structured–unstructured mesh of approximately 100k grid elements is adopted to guarantee a value of $y^+ \approx 1$ all along the blade surface and the solution almost independence from the number of elements. Figure 10 displays the mesh convergence study for the problem at hand. A grid with approximately 100k is deemed sufficient for optimization purposes. The Spalart–Allmaras

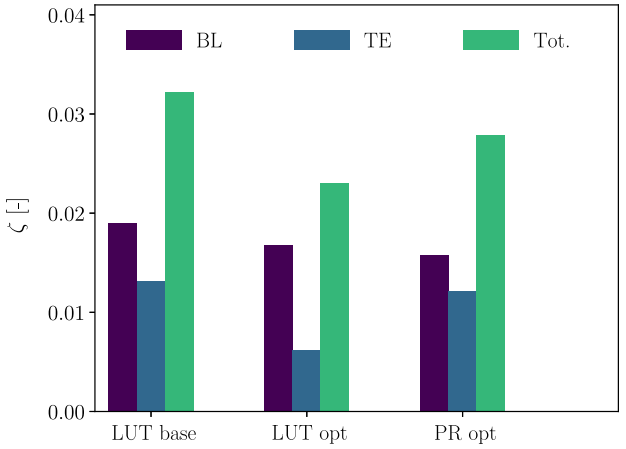

a) Fluid dynamic loss breakdown in terms of dimensionless kinetic energy loss coefficient ζ (Tot. = TE + BL). Quantities calculated as time-averaged values of the resolved time instances

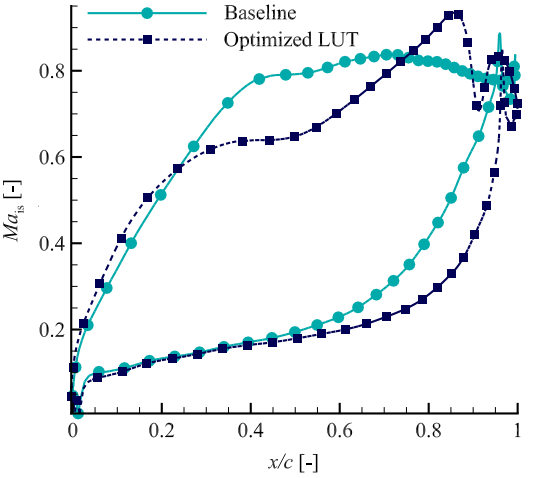

b) Isentropic mach number distribution along the baseline and *LUT*-based optimized blade surface for the first time instance

Fig. 8 Fluid-dynamic performance of the baseline and optimized LS-89 cascade.

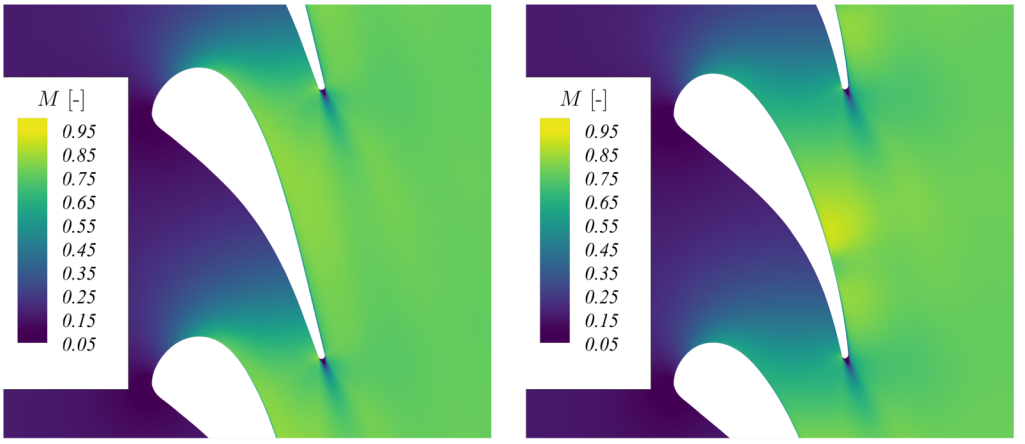

a) Baseline - $t = 0$ b) Optimized - $t = 0$

Fig. 9 Mach number contours plot obtained from harmonic balance simulations using the baseline and LUT-based optimized blade profiles at the first time instance.

Table 4 Main simulation parameters of the axial ORC turbine stage

Parameter	Value	Unit
Total inlet reduced temperature	1.1	—
Total inlet reduced pressure	0.8	—
Expansion ratio	1.5	—
Inlet turbulent intensity	5%	—
Turbulent viscosity ratio	100	—
Fluid molecular mass	114	kg/kmol
Specific heat ratio in dilute-gas limit (γ)	1.22	—
Dynamic viscosity	1.716×10^{-5}	kg/(m · s)
Thermal conductivity	0.0253	W/(m · K)

turbulence closure is used in this case to reduce the computational cost. A second-order accurate Roe scheme [25] is used in combination with the MUSCL approach and gradient limitation. The HB-based simulation results are computed for one single input frequency, i.e., the blade passage frequency, as this number was found to be the optimal tradeoff between accuracy of results and computational cost for design purposes. Note that the current implementation of the ug-LUT algorithm in SU2 does not yet allow the shape optimization of multirow turbomachinery. Because of this limitation, the stage optimization is based on PR with the constant γ value reported in Table 4.

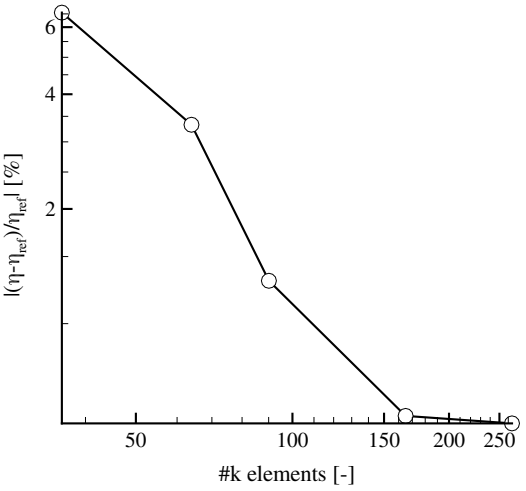

Fig. 10 Mesh independence study of the ORC axial stage test case.

The DVs are the 84 control points of the FFD boxes highlighted in Fig. 11. Figure 12 shows the optimization evolution of the dimensionless entropy generation and power. Additionally, in Fig. 12,

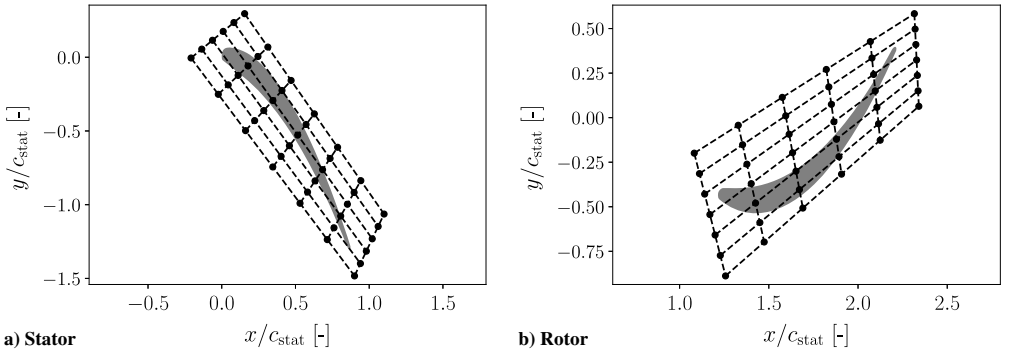

Fig. 11 Free-form deformation box and design variables.

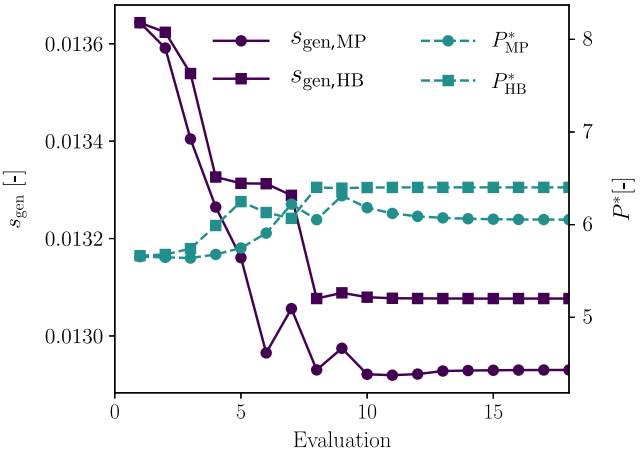

Fig. 12 Optimization history of the ORC axial stage obtained by using the mixing-plane (MP) and the harmonic balance (HB) method.

the results from a steady-state optimization in which the blade-row interface is modeled by means of the mixing-plane (MP) method are reported. Figure 13 depicts the baseline and the optimized blade shapes resulting from both the steady and the unsteady-based optimization. As can be observed, the resulting stators are characterized by largest shape differences, and in particular as a result of the considerable difference in the outlet camber angle. It can therefore be inferred that the two optimization methods may lead to significantly different stage designs, with possibly large implications in terms of stage fluid-dynamic performance.

The HB-based optimization leads to a reduction in the computed entropy generation by 4.2%, whereas for the MP-based optimization a decrease by 5.2% is observed. However, if the MP-based optimized blade profiles are employed in a HB simulation, the decrease in entropy is approximately 1.2%. Furthermore, the HB-based optimization leads to a power output higher by 5.4% if compared with the MP-based optimization results. From these findings, it can be inferred that the use of unsteady automated design methods could provide a step change in the fluid-dynamic performance of turbomachinery partly operating in the nonideal fluid regime.

Figure 14 shows the Mach number contours obtained from HB simulations of the flow around the baseline and the LUT-based optimized stage geometries at the first time instance. It can be observed in the optimized stage a significant reduction of the flow speed along the stator suction side, which results in a decrease of profile losses.

V. Conclusions

This paper documents the application of a fully turbulent adjoint method to the unsteady design optimization of turbomachinery working in the nonideal flow regime. The effectiveness of the method was demonstrated by performing a two-dimensional constrained shape optimization of two exemplary turbomachinery test cases operating in the nonideal flow regime: 1) a stator subject to a periodic inlet working condition; 2) a two-dimensional axial stage of an ORC power system.

Based on the outcomes of the study, it can be concluded that the proposed discrete adjoint-based harmonic balance method provides accurate sensitivities in comparison with second-order finite differences, if complex thermodynamic models are adopted or if the requested thermodynamic properties are computed via lookup tables. Furthermore, the combination of the HB-based adjoint and the use of thermodynamic models based on lookup tables enables efficient multirow shape optimization of turbomachinery operating in the nonideal flow regime. The computational cost of calculating the gradient of the objective function of interest with lookup tables is very similar to that involved when adopting the ideal gas model.

The method allows one to attain substantial efficiency gain for NICFD turbomachinery. In particular, the accuracy of the adopted thermodynamic model has an impact on the optimized blade profiles. For the analyzed turbine stator, the optimization using the thermodynamic model based on an equation of state (EoS) in the Span–Wagner functional form led to approximately 8% higher fluid-dynamic performance if compared with the optimization based on

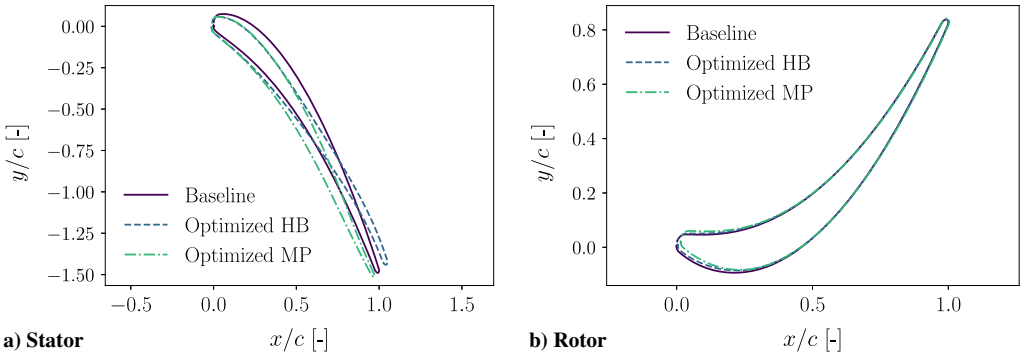

Fig. 13 Results of the shape optimization for the ORC turbine stage.

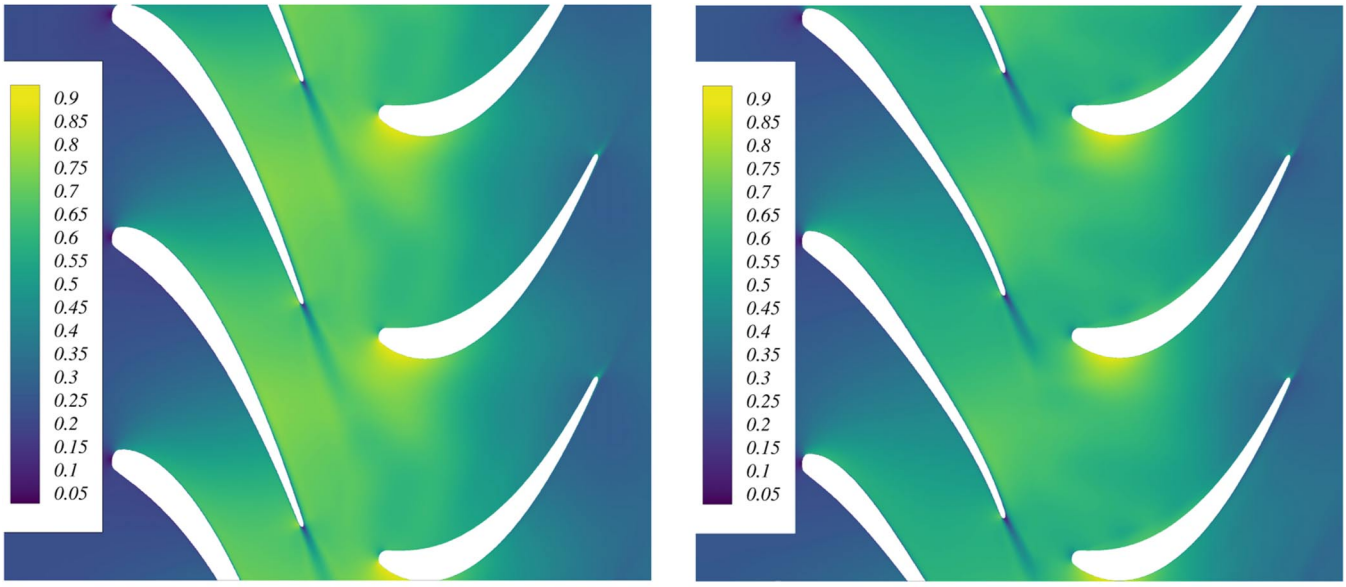

a) Baseline - $t = 0$ b) Optimized - $t = 0$

Fig. 14 Mach number contours plot obtained from harmonic balance simulations using the baseline and the PR-based optimized blade profiles at the first time instance.

a cubic EoS. This confirms the importance of adopting very accurate, thus complex, thermophysical fluid models for the optimization of cascades partly operating in the nonideal fluid regime.

The use of the unsteady-based optimization method for unconventional turbomachinery optimization enables to achieve higher fluid-dynamic performance if compared with the optimization based on steady-state methods. For the ORC turbine stage, the unsteady optimization led to an entropy generation reduction of 4.2%, whereas the steady-state optimization led a decrease of 1.2%. Furthermore, the output power of the HB-optimized stage increased by 5.4% relative to the one optimized by means of a mixing-plane method.

Summarizing, the findings of the study show that unsteady shape optimization of unconventional turbomachinery stages can be performed at affordable computational cost and that shape optimization based on unsteady flow models can provide a step forward in fluid-dynamic performance of such machines. The method thus offers interesting prospects for the design of innovative NICFD turbomachinery configurations. Future efforts will be therefore devoted to extend the multirow shape optimization method to 3D blade geometries and to the computation of thermophysical fluid properties via lookup tables with the final objective of systematically applying the resulting design method to obtain best design practices.

Appendix: Polytropic Peng–Robinson Thermodynamic Model

The PR thermodynamic model of a simple compressible substance is based on the volumetric and cubic equation of state

$$p(T, v) = \frac{RT}{v - b} - \frac{a\alpha^2(T)}{v^2 + 2bv - b^2} \tag{A1}$$

and on the assumptions $c_{P_0} = \text{const}$, $c_{v_0} = \text{const}$. Here, c_{P_0} and c_{v_0} are the ideal specific heat at constant pressure and volume; R is the gas constant; $v = 1/\rho$ the specific volume; and T the static temperature.

In the cubic equation of state, $\alpha(T)$ is related to the intermolecular attraction force, which depends on the temperature T, whereas a and b are temperature independent. These values are calculated as follows:

$$\begin{cases} a = 0.45724 \frac{(RT_{\text{cr}})^2}{P_{\text{cr}}} \\ b = 0.0778 \frac{RT_{\text{cr}}}{P_{\text{cr}}} \\ \alpha(T, \omega) = \left[1 + k\left(1 - \sqrt{\frac{T}{T_{\text{cr}}}}\right)\right] \\ k = \begin{cases} 0.37464 + 1.54226\omega - 0.26992\omega^2, & \omega \le 0.49 \\ 0.379642 + 1.48503\omega - 0.164423\omega^2 + 0.016666\omega^3, & \omega > 0.49 \end{cases} \end{cases} \tag{A2}$$

where T_{cr} and P_{cr} are the fluid critical temperature and pressure, and ω is the acentric factor. More details of the equation of state models can be found in [10].

The specific internal energy and specific entropy are given by

$$\begin{cases} e(T, v) = c_{v_0} T - \frac{a\alpha(T)(k+1)}{b\sqrt{2}} \tanh^{-1} \frac{b\sqrt{2}}{v+b} \\ s(T, v) = c_{v_0} \ln T + R \ln(v - b) - \frac{a\alpha(T)k}{b\sqrt{2T \cdot T_{\text{cr}}}} \tanh^{-1} \frac{b\sqrt{2}}{v+b} \end{cases} \tag{A3}$$

Acknowledgments

This research was supported by the Dutch Technology Foundation TTW, Applied Science Division of NWO, and the Technology Program of the Ministry of Economic Affairs, and by Bosch Corporate Research (Grant No. 13385). The SU2 software used in this work can be downloaded at https://github.com/arubino/SU2/tree/feature_testLUT.

References

[1] Colonna, P., Casati, E., Trapp, C., Mathijssen, T., Larjola, J., Turunen-Saaresti, T., and Uusitalo, A., "Organic Rankine Cycle Power Systems: From the Concept to Current Technology, Applications, and an Outlook to the Future," *Journal of Engineering for Gas Turbines and Power*, Vol. 137, No. 10, 2015, p. 19. https://doi.org/10.1115/1.4029884

[2] Kim, Y., Kim, C., and Favrat, D., "Transcritical or Supercritical CO_2 Cycles Using Both Low- and High-Temperature Heat Sources," *Energy*, Vol. 43, No. 1, 2012, pp. 402–415. https://doi.org/10.1016/j.energy.2012.03.076

[3] Ahamed, J., Saidur, R., and Masjuki, H., "A Review on Exergy Analysis of Vapor Compression Refrigeration Systems," *Renewable and Sustainable Energy Reviews*, Vol. 15, No. 3, 2011, pp. 1593–1600. https://doi.org/10.1016/j.rser.2010.11.039

[4] Kunick, M., Kretzschmar, H.-J., di Mare, F., and Gampe, U., "CFD Analysis of Steam Turbines with the IAPWS Standard on the Spline-Based Table Look-Up Method (SBTL) for the Fast Calculation of Real Fluid Properties," *ASME Turbo Expo 2015: Turbine Technical Conference and Exposition*, American Soc. of Mechanical Engineers Paper V008T26A037, New York, 2015, p. 10. https://doi.org/10.1115/GT2015-43984

[5] Congedo, P. M., Corre, C., and Cinnella, P., "Numerical Investigation of Dense-Gas Effects in Turbomachinery," *Computers and Fluids*, Vol. 49, No. 1, 2011, pp. 290–301. https://doi.org/10.1016/j.compfluid.2011.06.012

[6] Pasquale, D., Ghidoni, A., and Rebay, S., "Shape Optimization of an Organic Rankine Cycle Radial Turbine Nozzle," *Journal of Engineering for Gas Turbines and Power*, Vol. 135, No. 4, 2013, p. 13. https://doi.org/10.1115/1.4023118

[7] Persico, G., Rodriguez-Fernandez, P., and Romei, A., "High-Fidelity Shape Optimization of Non-Conventional Turbomachinery by Surrogate Evolutionary Strategies," *Journal of Turbomachinery*, Vol. 141, No. 8, 2019, p. 11. https://doi.org/10.1115/1.4043252

[8] Vitale, S., Albring, T. A., Pini, M., Gauger, N. R., and Colonna, P., "Fully Turbulent Discrete Adjoint Solver for Non-Ideal Compressible Flow Applications," *Journal of the Global Power and Propulsion Society*, Vol. 1, Nov. 2017, pp. 252–270. https://doi.org/10.22261/JGPPS.Z1FVOI

[9] Pini, M., Persico, G., Pasquale, D., and Rebay, S., "Adjoint Method for Shape Optimization in Real-Gas Flow Applications," *Journal of Engineering for Gas Turbines and Power*, Vol. 137, No. 3, 2015, p. 13. https://doi.org/10.1115/1.4028495

[10] Vitale, S., "Advancements in Automated Design Methods for NICFD Turbomachinery," Ph.D. Thesis, Delft Univ. of Technology, Delft, The Netherlands, 2018.

[11] Palacios, F., Alonso, J., Duraisamy, K., Colonno, M., Hicken, J., Aranake, A., Campos, A., Copeland, S., Economon, T., Lonkar, A., et al., "Stanford University Unstructured (SU2): An Open-Source Integrated Computational Environment for Multi-Physics Simulation and Design," *51st AIAA Aerospace Sciences Meeting Including the New Horizons Forum and Aerospace Exposition*, Vol. 287, AIAA Paper 2013-0287, 2013. https://doi.org/10.2514/6.2013-287

[12] Economon, T. D., Palacios, F., Copeland, S. R., Lukaczyk, T. W., and Alonso, J. J., "SU2: An Open-Source Suite for Multiphysics Simulation and Design," *AIAA Journal*, Vol. 54, No. 3, 2015, pp. 828–846. https://doi.org/10.2514/1.J053813

[13] Rubino, A., Pini, M., Colonna, P., Albring, T., Nimmagadda, S., Economon, T., and Alonso, J., "Adjoint-Based Fluid Dynamic Design Optimization in Quasi-Periodic Unsteady Flow Problems Using a Harmonic Balance Method," *Journal of Computational Physics*, Vol. 372, Nov. 2018, pp. 220–235. https://doi.org/10.1016/j.jcp.2018.06.023

[14] Rubino, A., Vitale, S., Colonna, P., and Pini, M., "Fully-Turbulent Adjoint Method for the Unsteady Shape Optimization of Multi-Row Turbomachinery," *Aerospace Science and Technology*, Vol. 106, Nov. 2020, Paper 106132. https://doi.org/10.1016/j.ast.2020.106132

[15] Rubino, A., Pini, M., Kosec, M., Vitale, S., and Colonna, P., "A Look-Up Table Method Based on Unstructured Grids and Its Application to Non-Ideal Compressible Fluid Dynamic Simulations," *Journal of Computational Science*, Vol. 28, Sept. 2018, pp. 70–77. https://doi.org/10.1016/j.jocs.2018.08.001

[16] Colonna, P., Van der Stelt, T., and Guardone, A., "FluidProp (Version 3.1): A Program for the Estimation of Thermo Physical Properties of Fluids," *A Computer Program Since 2004*, Delft Univ. of Technology, Delft, The Netherlands, 2019, http://www. FluidProp.com.

[17] Donea, J., Huerta, A., Ponthot, J.-P., and Rodriguez-Ferran, A., "Arbitrary Lagrangian-Eulerian Methods," *Encyclopedia of Computational Mechanics*, edited by E. Stein, R. Borst, and T. J. Hughes, Wiley, New York, 2004, Chap. 14. https://doi.org/10.1002/0470091355.ecm009

[18] Menter, F. R., "Zonal Two Equation k-ω, Turbulence Models for Aerodynamic Flows," *Fluid Dynamics and Co-Located Conferences*, AIAA Paper 1993-2906, 1993.

[19] Sagebaum, M., Albring, T., and Gauger, N. R., "High-Performance Derivative Computations Using CoDiPack," *ACM Transactions on Mathematical Software*, Vol. 45, No. 4, Dec. 2019.

[20] Saxer, A. P., "A Numerical Analysis of 3-D Inviscid Stator/Rotor Interactions Using Non-Reflecting Boundary Conditions," Gas Turbine Lab., Massachusetts Inst. of Technology, Tech. Rept. GTL-209GTL, Cambridge, MA, 1992.

[21] Kraft, D., "A Software Package for Sequential Quadratic Programming," DLR German Aerospace Center—Institute for Flight Mechanics, Dfvlr-fb 88-28, Germany, 1988.

[22] Mee, D. J., Baines, N. C., Oldfield, M. L. G., and Dickens, T. E., "An Examination of the Contributions to Loss on a Transonic Turbine Blade in Cascade," *Journal of Turbomachinery*, Vol. 114, No. 1, 1992, pp. 155–162. https://doi.org/10.1115/1.2927979

[23] Denton, J. D., and Xu, L., "The Trailing Edge Loss of Transonic Turbine Blades," *Journal of Turbomachinery*, Vol. 112, No. 2, 1990, pp. 277–285. https://doi.org/10.1115/1.2927648

[24] Denton, J. D., "The 1993 IGTI Scholar Lecture: Loss Mechanisms in Turbomachines," *Journal of Turbomachinery*, Vol. 115, No. 4, 1993, pp. 621–656. https://doi.org/10.1115/1.2929299

[25] Roe, P. L., "Approximate Riemann Solvers, Parameter Vectors, and Difference Schemes," *Journal of Computational Physics*, Vol. 43, No. 2, 1997, pp. 357–372. https://doi.org/10.1006/jcph.1997.5705

J. P. Bons
Associate Editor